Atmos. Chem. Phys. Discuss., 14, 28105–28146, 2014
www.atmos-chem-phys-discuss.net/14/28105/2014/
doi:10.5194/acpd-14-28105-2014

Atmospheric Chemistry and Physics Discussions

Atmospheric brown clouds reach the Tibetan Plateau by crossing the Himalayas

Z. L. Lüthi[1], B. Škerlak[2], S.-W. Kim[3], A. Lauer[4], A. Mues[4], M. Rupakheti[4], and S. Kang[5,1]

[1]Key Laboratory of Tibetan Environment Changes and Land Surface Processes, Institute of Tibetan Plateau Research and CAS Center for Excellence in Tibetan Plateau Earth Sciences, Chinese Academy of Sciences (CAS), Beijing, China
[2]ETH Zurich, Institute for Atmospheric and Climate Science, Zürich, Switzerland
[3]School of Earth and Environmental Sciences, Seoul National University, Seoul, Republic of Korea
[4]IASS Institute for Advanced Sustainability Studies, Potsdam, Germany
[5]State Key Laboratory of Cryospheric Science, Cold and Arid Regions Environmental and Engineering Research Institute, CAS, Chinese Academy of Sciences, Lanzhou, China

Received: 20 August 2014 – Accepted: 22 October 2014 – Published: 13 November 2014

Correspondence to: Z. L. Lüthi (zoe.luethi@iass-potsdam.de) and
S. Kang (shichang.kang@lzb.ac.cn)

Published by Copernicus Publications on behalf of the European Geosciences Union.

ACPD
14, 28105–28146, 2014

Abstract

The Himalayas and the Tibetan Plateau region (HTP), despite being a remote and sparsely populated area, is regularly exposed to polluted air masses with significant amounts of aerosols including black carbon. These dark, light-absorbing particles are known to exert a great melting potential on mountain cryospheric reservoirs through albedo reduction and radiative forcing. This study combines the available yet sparse ground-based and satellite data to identify a severe aerosol pollution episode observed simultaneously in central Tibet and on the southern side of the Himalayas during 13–19 March 2009. We detail how polluted air masses such as an atmospheric brown cloud (ABC) over South Asia reached the Tibetan Plateau during this pre-monsoon case study. In order to address the mechanisms of pollution transport in the complex topography of the HTP, air-mass trajectories are calculated using hourly outputs from the high-resolution numerical weather prediction model COSMO. Cross-mountain pollution transport is found to occur to a large extent at elevated tropospheric levels other than just through major river valleys. Lifting and advection of polluted air masses over the great mountain range is enabled by a combination of synoptic and local meteorological settings. Winds over the Indo Gangetic Plain (IGP) are generally weak at lower levels during the event, allowing for accumulation of pollutants. The passing of synoptic-scale troughs leads to south-westerly flow in the middle troposphere over northern and central India. Thus, ABC can build up south of the Himalayas and get carried northwards across the mountain range and onto the Tibetan Plateau as the winds obtain a southerly component. Air masses from the ABC hot-spot of the IGP can reach the high glaciers, which may have serious implications for the cryosphere in the HTP region and for climate on regional to global scales.

ACPD
14, 28105–28146, 2014

1 Introduction

The Himalayas and Tibetan Plateau region (HTP), sometimes called the Third Pole, represent key areas with the largest volume of ice outside the polar regions that impact radiative budgets and climate (Ye and Wu, 1998; Ma et al., 2009). Recently, a growing body of research has demonstrated that the HTP atmosphere and cryosphere are undergoing extraordinary changes, including atmospheric warming (Gautam et al., 2010; Thompson et al., 2000; Kang et al., 2010) and in many parts rapid glacier melting (Bolch et al., 2012; Yao et al., 2012). Consequently, the seasonal water availability of important Asian river systems are very likely to be affected (Immerzeel et al., 2010; Kehrwald et al., 2008). In addition to greenhouse gases, increasing ambient concentrations of black carbon (BC) appear to be an anthropogenic driving force of the observed changes in these remote regions (Lau et al., 2010; Ramanathan and Carmichael, 2008). Light-absorbing aerosol particles such as mineral dust and BC contribute to the atmospheric heating and the albedo reduction once deposited on glaciers. Albeit only contributing a few percent to the total aerosol mass, BC exerts major radiative effects (Bond et al., 2013; Jacobson, 2001), especially over the HTP during pre-monsoon seasons when the solar radiative flux at the surface is very high (Flanner et al., 2007).

Even though background air pollution levels in the HTP region are very low, recurring pre-monsoonal BC peaks have been documented at high altitudes of the south-facing Himalayan slopes (e.g., Marinoni et al., 2010, 2013; Decesari et al., 2010) which are sometimes directly exposed to atmospheric brown clouds (ABC) (Ramanathan et al., 2007b; Bonasoni et al., 2010). Brown clouds have been defined as "huge blankets or layers of *haze* generally composed of light-absorbing submicrometer-sized carbonaceous aerosol particles" (Engling and Gelencser, 2010). Areas that are particularly affected by brown clouds, so-called ABC hot-spots, are characterized by an anthropogenic aerosol optical depth (AOD) larger than 0.3 and an absorbing aerosol optical depth (AAOD) greater than 0.03 for at least one season (Ramanathan et al., 2007a). Such conditions are frequently observed on the southern side of the Himalayas, espe-

ACPD
14, 28105–28146, 2014

cially over the Indo Gangetic Plain (IGP) during the dry months (November to May). BC transported from this regional hot-spot might thus contribute to the retreat of Himalayan glaciers (Engling and Gelencser, 2010). Furthermore, recent studies show BC observations on snow and in ice even further north on the Tibetan Plateau (TP) (e.g., Xu et al., 2009; Qian et al., 2011; Ming et al., 2013; Kaspari et al., 2011). Engling et al. (2011) and Xia et al. (2011) report springtime episodes with large amounts of pollutants observed on the TP. As a consequence of such episodes, BC concentrations on glaciers could significantly increase on the TP and consequently affect the surface albedo (Zhao et al., 2013).

Recent GEOS-Chem and HYSPLIT model calculations of BC advection to the TP suggest that the dominant source regions depend on season and receptor location but South and East Asia show the highest overall contribution (Kopacz et al., 2011; Lu et al., 2012). However, to date, the mechanisms of pollutant transport from the IGP hot-spot and from the foothills of the Himalayas to the TP have not been investigated in detail. A widespread hypothesis published by Cao et al. (2011) suggests that the high altitude of the Himalayas acts as a physical barrier, inhibiting the transport of BC across the mountains onto the TP with the exception of deep river valleys that cut across the Himalayas providing a pathway for pollutant transport.

One reason for the limited knowledge about aerosol pollution on the HTP is the small number of long-term in-situ observations in this highly complex topography with its very specific meteorology. In addition, the results from chemistry transport models still have large uncertainties, as do the emission datasets that are used for modeling (Fleming et al., 2012).

The present work addresses the mechanisms and pathways of cross-Himalayan pollution transport that occurs over large areas under specific meteorological conditions. We base the analysis on the pollution event in March 2009 that can be identified from ground-based and space-borne remote sensing data (Sect. 3.1). We present trajectory calculations and an analysis of the meteorological situation using a regional high-resolution numerical weather prediction model (Sects. 3.2 and 3.3). The goals of this

ACPD
14, 28105–28146, 2014

study are: (1) to investigate whether major pollution episodes identified on the TP set in synchronously with pollution episodes measured at the southern face of the Himalayas, (2) to determine if "plumes" of air pollution observed on the TP originate at the southern side of the Himalayas, (3) to determine whether ABC measured at the southern side of the Himalayas can traverse the high mountain range not only through the major north–south river valleys but also by being lifted and advected over the Greater Himalayas, (4) to understand which local and synoptic-scale meteorological phenomena enable the transport across the Himalayas.

The aim of this work is to improve the understanding of the intensely discussed cross-Himalayan air pollution transport and its effect on the cryosphere and the climate, in the context of raising anthropogenic emissions in Asia.

2 Methods and data

The two HTP reference stations for the cross-Himalayan pollution transport are Nam Co Monitoring and Research Station for Multisphere Interactions (Nam Co), situated in central Tibet (30.77° N, 90.96° E, 4730 m a.s.l.) and EvK2-CNR Nepal Climate Observatory-Pyramid (EvK2) located at the southern face of the Greater Himalayas (27.95° N, 86.81° E, 5050 m a.s.l.) as shown in Fig. 1.

Detailed analysis are presented for the episode of 13–19 March 2009, which was identified as the most severe event showing highest yearly anthropogenic aerosol amounts at Nam Co with simultaneous observations at EvK2.

2.1 Ground-based data

The identification of aerosol pollution events that occurred in the HTP region are based on quality assured data from the Aerosol Robotic Network (AERONET) (Holben et al., 1998). AERONET provides globally distributed observations of spectral aerosol optical depth (AOD), inversion products, and the amount of precipitable water. Complete

ACPD
14, 28105–28146, 2014

descriptions of the sun-sky scanning spectral radiometer instruments, measurement sequences, uncertainties and cloud screening procedures can be found in the literature (e.g., Eck et al., 1999; Dubovik and King, 2000; Smirnov et al., 2000). In this study only datasets that have the lowest possible uncertainties in unpolluted regions are used. We therefore do not include spectral refractive indices and single scattering albedo from almucantar scans with AOD (440 nm) < 0.4 to ensure sufficient sensitivity to aerosol absorption (Dubovik et al., 2000). We thus use results from the Spectral Deconvolution Algorithm (SDA) version 2, level 2.0, which uses optical principles to distinguish the submicron fine-mode AOD (hereafter FMF) from the super-micron coarse mode AOD at a standard wavelength of 500 nm (O'Neill, 2003).

Here, FMF is taken as a proxy for polluted air since anthropogenic aerosol optical thickness is dominated by fine aerosol, while natural aerosols contain a substantial fraction of coarse aerosols. Typically the radius of these coarse particles is > 1 µm as they are being generated mechanically such as mineral dust and sea salt, while combustion-produced particles including open burning, biofuel use and industrial pollution are predominately fine mode particles with a radius of < 1 µm (Eck et al., 2010).

At Nam Co, over 680 days of level 2 SDA data were available at the time of this study, covering the years 2006–2012. This site is a representative background station and it represents the only AERONET site with long-term L2 datasets in central Tibet at the time of this study; Nam Co is well suited to assess the extent and effect of long-range transport of pollution to inland TP (Xia et al., 2011; Cong, 2009). Datasets from additional AERONET sites (see Fig. 1) with level 2 SDA data available for the time period of the most severe pollution event are used in order to examine the spatial pollution extent. We define pollution events as periods with at least five days showing high FMF (i.e. daily means that lie in the 75th percentile) simultaneously at Nam Co and at EvK2. Details about the AERONET stations are presented at http://aeronet.gsfc.nasa.gov from where all quality assured data have been downloaded.

ACPD
14, 28105–28146, 2014

2.2 Satellite data

Cloud-Aerosol Lidar with Orthogonal Polarization (CALIOP) is a two-wavelength polarization-sensitive lidar on board of the Cloud-Aerosol Lidar and Infrared Pathfinder Satellite Observation (CALIPSO) satellite. Its datasets provide high-resolution vertical profiles of aerosols and clouds at a 16 day revisiting time. Night-time profiles show lower background noise, which is an advantage when analyzing pollution aerosols in remote areas such as the HTP. Detailed information about the instrument, data resolution, measurement techniques and final products are given by Winker et al. (2009). For this study, we selected nighttime profiles upwind of the HTP AERONET stations during the pollution event in order to analyze the vertical extension of polluted air masses that are transported towards the HTP. The products used in this study include the following datasets: level 1B total (Parallel and Perpendicular) attenuated backscatter ($km^{-1}\,sr^{-1}$) showed in color-modulated, altitude-time images at 532 nm; lidar level 2 Vertical Feature Mask which distinguishes between clouds and aerosol (based on the Cloud Aerosol Discrimination (CAD) function) and an aerosol subtype identification which is also a level 2 product based on the Scene Classification Algorithm (SCA) (Winker et al., 2009).

Aerosol absorption optical depth (AAOD) is calculated with the near-UV OMAERUV algorithm for measurements by the Ozone Monitoring Instrument (OMI) aboard the Aura satellite (Torres et al., 2007). Two AAOD 500 nm datasets are used in this study in order to compare the light-absorbing aerosol distribution over southern Asia during the analyzed pollution event and during a "cleaner" period over the HTP and over the IGP.

2.3 Analysis of air mass history

Due to the complex topography of the HTP region, a detailed analysis of the history of polluted air masses requires high-resolution meteorological fields. To this end, we performed a 7 day simulation with the non-hydrostatic numerical weather prediction (NWP)

ACPD
14, 28105–28146, 2014

model COSMO (Baldauf et al., 2011) from 00:00 UTC 10 March 2009 to 00:00 UTC 17 March 2009. The model was run at a horizontal resolution of 7 km (0.0625°, rotated grid) and with 79 vertical levels from the surface up to 15 hPa. The internal model time step is 40 s and meteorological fields are written to disk every hour. COSMO is driven by operational analyses from the European Centre for Medium-Range Weather Forecasts (ECMWF, 0.5° horizontal resolution and 91 vertical levels) which are used to update the boundary conditions every 6 h.

Kinematic backward and forward trajectories were calculated using the Lagrangian Analysis Tool LAGRANTO (Wernli and Davies, 1997), which applies an iterative Eulerian integration scheme (3 steps) to the hourly wind fields from COSMO. Two ensembles of trajectories were started in this study: the first one (48 h backward and forward) at 21:00 UTC 13 March 2009 over an aerosol-rich air mass in Tibet and the second one (72 h backward at 03:00 UTC 16 March 2009) over Nam Co station. In both cases, we started sets of 121 trajectories at a horizontal distance of less than 60 km at various heights from the surface to 2000 m above ground (in steps of 100 m). Meteorological parameters such as temperature and water vapor mixing ratio from COSMO outputs are interpolated in time and space to the trajectory location.

3 Results and discussion

In this section, we examine the severe pollution episode of 13–19 March 2009 as a case study. To this end we analyze: (1) AERONET time-series and compare them to BC observational data from sites in the HTP region and to OMI AAOD data in order to select the cross-Himalayan pollution event and assess the ABC extension, (2) a CALIOP vertical cross section from the IGP to inland Tibet showing a pollution "plume" over the TP; 48 h backward and forward trajectories are calculated to determine whether the plume originates south of the Himalayas and whether it is carried towards Nam Co, (3) 72 h back-trajectories from Nam Co on the day with greatest FMF observed in Tibet

ACPD
14, 28105–28146, 2014

demonstrating how ABC can cross the Himalayas, (4) meteorological conditions that favor the formation of severe air pollution and the long-range transport onto the HTP.

3.1 Air quality measurements in the HTP region

Only for the years 2009 and 2010 complete 24 months of AERONET L2 measurements at Nam Co are available. These measurements show significant episodes of fine-mode aerosol contribution to total AOD 500 nm during the pre-monsoon months. Interestingly, the most remarkable episodes were found to occur synchronously with high FMF observations at EvK2 station. The FMF AOD 500 nm is mostly associated with pollution aerosols which mainly consist of particles in the submicron fraction (cfr. Sect. 2.1). Over the course of 2009 and 2010, eight cross-Himalayan pollution events were identified during the months of March, April and May. Here we present details of the most severe pollution episode, it occurred on 13–19 March 2009 (Fig. 2). This event shows an average FMF at Nam Co of 0.2, the mean of the remaining seven events range from 0.03 to 0.07. Overall, the case study contributed with 15 % to the yearly pollution occurrence at Nam Co in 2009–2010 and 20 % in the year 2009.

The AERONET fine-mode AOD (500 nm) and the total AOD (500 nm) for Nam Co and EvK2 during March and April 2009 (Fig. 2) suggest an increase of FMF in mid-March (gray bar) and a subsequent cleaner period in the end of March (blue bar). A sudden rise in the FMF occurred at EvK2 on 13 March 2009 and one day later at Nam Co. The pollution levels at the two HTP stations stayed elevated until 19 March 2009. No AERONET data is available for 15 March 2009, which was an overcast day and thus sun-sky radiometer measurements could not be performed.

The maximum FMF (500 nm) at Nam Co peaked at 0.38 on 16 March 2009. This is consistent with the findings of Xia et al. (2011) who reported that the total AOD 500 nm at Nam Co was at its maximum on this day with a value of 0.42, one order of magnitude above average conditions at this Tibetan station (annual baseline = 0.029). We present details in Sects. 3.2 and 3.3 about cross-Himalayan pollution transport based on high

ACPD
14, 28105–28146, 2014

resolution trajectory calculations for the days with very high FMF at Nam Co, i.e. 14 and 16 March 2009.

In order to further support the association of FMF with pollution aerosols and in particular with absorbing aerosols we compare the AERONET data with available in-situ BC concentrations. The BC data were retrieved from Multi-Angle Absorption Photometer measurements and from filter analyses at EvK2 and at Nam Co station, respectively. The circles in Fig. 2 show a high temporal correlation of BC concentrations with the FMF at EvK2 station. Continuous BC measurements at Nam Co station are only available since late 2010 (M. Jing, personal communication, 20 November 2013) but a recent study on total suspended particulate matter by Zhao et al. (2013) points out that a sudden increase of carbonaceous aerosols, i.e. organic carbon and black carbon, also occurred in mid-March 2009 (not shown). These in situ data suggest that this pre-monsoon aerosol event consisted of significant pollution which reached central Tibet not only at elevated levels but also at the surface.

The extraordinarily high FMF at Nam Co relative to EvK2 during this 2009 event suggests the possible formation of new fine particles from precursor gases and subsequent growth during the long-rage transport of polluted air masses. New particle formation by nucleation is particularly effective under low relative humidity and high solar radiation which are typical characteristics of the HTP in the pre-monsoon season. Moorthy et al. (2011) have observed this phenomena at a trans-Himalayan high-altitude location and stated that new particle formation plays a dominant role in controlling the particle size distribution and concentrations in this region.

3.1.1 ABC determination

A significant buildup of air pollution during the 13–19 March 2009 event was also observed at stations over the IGP and in northern Thailand. AERONET sites with available L2 data during the case study are shown in Fig. 3 (see Fig. 1 for the location of the stations). Interestingly, compared to EvK2 station in Fig. 2, the AERONET measurements from the IGP show a relatively large contribution of coarse mode particles to the total

ACPD
14, 28105–28146, 2014

AOD 500 nm, which is mostly associated with wind-blown dust. This is in line with the results of Prabha et al. (2012), Gautam et al. (2011) and Dey and Di Girolamo (2010), who have recently reported a larger contribution of dust aerosols to total AOD over the IGP compared to the southern slope of the Himalayas, where fine-mode anthropogenic pollution aerosols play a dominant role during the pre-monsoon. Yet, it is important to bear in mind that a significantly increasing trend of anthropogenic aerosols has been identified in data of the AERONET Ångström exponent over India especially during December to March as recently reported by Babu et al. (2013). This implies an increase in air pollution over the IGP during the past years.

Overall, the AERONET datasets in Figs. 2 and 3 suggests the occurrence of an ABC over South Asia that extends as far as the HTP. This is pointed out in the significant (nearly total) FMF contribution to the total AOD 500 nm at EvK2 station. A direct exposure of the station to ABC has recently been analyzed by the numerous studies with the comprehensive datasets from this high-altitude atmospheric monitoring site (e.g., Bonasoni et al., 2010; Decesari et al., 2010; Marinoni et al., 2013).

The high contribution of absorbing aerosols to the total AOD during the 13–19 March 2009 pollution event is shown in Fig. 4a with the OMI AAOD 500 nm. For comparison, Fig. 4b depicts the spatial distribution of AAOD during a "cleaner" 7 day period (30 March to 5 April 2009, see Figs. 2 and 3) in the region surrounding the HTP. The dense haze extending SW of the HTP displayed in Fig. 4a suggests the occurrence of an ABC with a significant amount of absorbing aerosols along the foothills of the Himalayas. The HTP region on the other hand appears as a blank area in Fig. 4. This is due to the fact that the satellite derived AAOD data are very limited for the HTP as a consequence of its high surface reflectance.

The combination of ground and space based remote sensing data suggests the presence of an ABC with AERONET AOD > 0.3 and OMI AAOD > 0.03 that were observed not only south of the great mountains or in the Himalayan valleys but also on the TP.

ACPD
14, 28105–28146, 2014

3.2 Air pollution features on the TP and their source regions

This section addresses the transport mechanisms of two major pollution features observed over the TP during the March 2009 event: (1) a polluted air mass or "plume" retrieved by CALIOP during the overpass of CALIPSO which was closest in time and distance upwind from Nam Co station on 13 March 2009 and (2) the highest daily FMF at Nam Co on 16 March 2009.

3.2.1 Plume (satellite data)

Several CALIOP transects retrieved over the past years show pollution aerosols that "coat" the HTP, indicating that the polluted air masses do not only accumulate in the valleys but can also cover large areas in this usually pristine region.

In Fig. 5 we show the CALIOP transect retrieved upstream of Nam Co station at 20:35 UTC 13 March 2009, during the onset of the pollution event analyzed in this study. Thin cirrus clouds can be seen at about 10 km (yellow to gray). A dense layer of aerosols extending over a vast area from India and Nepal to the TP, where it reaches elevations of 6–7 km a.s.l., is visible in the lidar backscatter data (Fig. 5a) and in the Cloud Aerosol Discrimination output (Fig. 5b). The aerosol layer over southern TP (red circle, hereafter referred to as "plume") was identified as air pollution through the CALIPSO aerosol subtype classification, and more specifically as carbonaceous particles or smoke aerosols (Fig. 5c).

In order to investigate how this plume reached the TP and where this polluted air is advected to, we calculated 48 h backward and forward trajectories (see Sect. 2.3) starting at 21:00 UTC 13 March 2009 in the vicinity of the observed plume (30.00° N, 86.15° E). Here we show the trajectories started near the surface at 5510 m a.s.l. (see Fig. 6). The trajectories started at higher altitudes do not show significant differences, indicating robust transport pathways throughout the lowermost 2000 m.

These backward trajectories suggest that the source region of the plume is located southwest of the Himalayas and that the transport occurs predominantly along a rela-

ACPD
14, 28105–28146, 2014

tively narrow band without much vertical motion (see color-coded height field in Fig. 6). Some of the backward trajectories, however, also originate from lower altitudes (about 2000 m) directly south of the Himalayas indicating strong uplifting and the transport of polluted air from the PBL over the northern IGP up to the plateau. Major valleys seem to play an important role for this subset as the trajectories are channeled through them. Interestingly, some of the trajectories actually originate from the TP, flow down through valleys to the IGP during nighttime where they can mix with polluted air and are then lifted onto the TP again during daytime (see also Sect. 3.3.1).

From the plume location, the polluted air is transported eastwards, which explains the remarkably high levels of fine-mode aerosols measured at Nam Co on the following day (14 March, see Fig. 2, data available from 01:00 to 07:00 UTC). This suggests that there is a direct connection between the CALIOP aerosol-rich air (plume) and the AERONET high FMF at Nam Co. Note the wide spread of heights of the trajectories in the vicinity of Nam Co, showing that the pollution is distributed throughout the whole troposphere, reaching levels of up to 10 000 m a.s.l. This could potentially allow for mixing of pollution into the stratosphere during stratosphere–troposphere exchange (STE) events, particularly since the TP region is known to be a hot spot for such events (Škerlak et al., 2014).

3.2.2 Nam Co (in-situ data)

In order to further investigate possible transportation pathways of air pollution across the Himalayas onto the TP we also calculated backward trajectories from the vicinity of the AERONET station Nam Co on the TP. The highest FMF contribution to total AOD during the pollution event was measured at 03:00 UTC 16 March 2009 (cf. Fig. 2). We therefore calculated 72 h backward trajectories arriving close to the surface at 4720 m a.s.l. near Nam Co (see Fig. 7). We find that most air masses originate south of the Himalayas and reach the plateau along two main crossings: one is over the Chumbi Valley between Sikkim, Bhutan and Tibet and one lies further to the East over central and eastern Bhutan. Air masses are also advected from comparatively

ACPD
14, 28105–28146, 2014

low altitudes (below 5000 m a.s.l.) and lifted across the Himalayas. Since the adjacent southern regions are highly polluted (compare Fig. 4a), this indicates an effective transport pathway for pollution including absorbing aerosols. Similar cross-mountain pathways were also observed in a study on trans-Himalayan flights of bar-headed geese by Hawkes et al. (2011).

The BC data from EvK2 show extraordinary high values of up to 3800 ng m^{-3} at 17:00 local Nepal time on 15 March 2009, one day before the high AOD values were measured at Nam Co. Together with the back-trajectory calculations discussed above, this supports the hypothesis that these polluted air masses were transported from EvK2 and its surroundings to Nam Co in less than 24 h. A detailed analysis of the involved air streams can be found in Sect. 3.3.2.

3.3 Transport mechanisms

We identify three transport pathways of air (hereafter referred to as "air streams") arriving at the plume region and Nam Co (see Sect. 3.2). These are further analyzed in this section in order to understand the transport mechanisms responsible for the cross-Himalayan flow.

3.3.1 Plume

In case of the plume region with high aerosol concentrations observed at 21:00 UTC 13 March 2009 (cf. Sect. 3.2.1), three major source regions of the air can be identified (see Fig. 8). A large fraction of the trajectories is advected over the Himalayas from the south-west and stay at approximately constant altitude. We refer to these trajectories as "air stream 1" (blue lines in Fig. 8) if they stay above 5500 m a.s.l. over the IGP and as "air stream 2" (green) otherwise. "Air stream 3" (orange) consists of trajectories that originate over the TP and cross the Himalayas from North to South before being lifted onto the TP again. Out of 121 trajectories started at 5510 m a.s.l., 117 (97 %) fall into one of these three categories. The three air streams contribute approximately equally

ACPD
14, 28105–28146, 2014

to the air in the vicinity of the observed aerosol plume with 36, 43 and 38 trajectories in air streams 1, 2 and 3, respectively. Air stream 3 was found to only contribute to near-surface air at the plume location whereas air streams 1 and 2 also appear in all backward trajectory calculations started at higher levels.

The temporal evolution of height, water vapor (Qv), potential temperature (θ) and equivalent potential temperature (θ_e) along the trajectories is shown in Fig. 9. The trajectories show that air streams 1 and 2 stay roughly at constant altitude (around 5500 m a.s.l.) throughout 12 March. Therefore, the advection can be estimated from the synoptic situation at 500 hPa. As can be seen from the geopotential height at 500 hPa shown in Fig. 10, a ridge over India results in westerly (north-westerly) winds over Northern (North-Eastern) India at mid-tropospheric levels. These winds obtain an increasing southerly component on 13 March as the ridge moves eastwards followed by a new trough. This results in a south-westerly flow over large parts of Northern India. As air streams 1 and 2 are advected towards the Himalayas quasi-isentropically on slanting isentropes, they rise approximately 1000 m when crossing the Himalaya (see Fig. 9).

All trajectories enter the PBL over the TP in the afternoon of 13 March (Fig. 9). As a consequence, water vapor content rises abruptly to values around 1 g kg^{-1}, which is also reflected in a θ_e increase. Away from the TP, potential temperature decreases with a rate in the order of 1 K day^{-1}, which is typical for radiative cooling of the free troposphere. Over the plateau, however, a strong decrease in θ from 316 to 312 K can be seen as the trajectories within the PBL over the TP are affected by radiative cooling of the surface during nighttime. Note that no diurnal cycle is visible in θ and θ_e on 12 March for trajectories in the free troposphere.

Air stream 3 descends from the TP on 12 March on the western side of the passing trough (see Figs. 6 and 10) to the southern side of the Himalayas. There, the air is first advected eastwards in the afternoon of 12 March before returning to west Nepal during the following night. This is consistent with the zonal winds along the southern face of the Himalayas at 850 hPa shown in Fig. 11 that change from westerlies on 12 March

ACPD
14, 28105–28146, 2014

to easterlies on 13 March as the new trough discussed above is approaching. During the night, vertical mixing is much weaker and valley wind systems seem to play an important role. At the southeastern corner of the TP, the prevailing northerly winds on the rear side of the passing trough are channeled by the Brahmaputra valley as they descend. Thus, even though winds at 500 hPa are still westerly, at lower levels, easterlies prevail over much of the IGP.

With the Himalayan flanks heating up during daytime on 13 March, air stream 3 rises approximately 2000 m within 10 h. As this air stream has been in contact with the PBL (or at least very near to its top) over the TP and the IGP, it is affected by the diurnal temperature cycle of the near surface air temperature near the surface which can be seen in the temporal evolution of θ and θ_e along the trajectories and the elevated values of Qv. On average, the potential temperature rises around 3 K on 12 March when most of the trajectories are above the TP and around 5 K as they ascend across the Himalayas on 13 March.

The very high PBL and the strong updrafts near the surface associated with the heated mountain flanks can be seen in a cross-section along the main flow direction (thick black line in Fig. 8) at 09:00 UTC 13 March 2009 (Fig. 12). While air streams 1 and 2 (blue and green squares, respectively) cross the Himalayas quasi-isentropically at approximately 500 hPa (approx. 318 K), air stream 3 is lifted from the PBL before joining the pathway of air stream 1 and 2. After crossing the Himalayas, the air streams continue to mix and merge.

The advection (air streams 1 and 2) and lifting (air stream 3) of air masses from the IGP to the TP is enabled by the large-scale forcing, i.e., the winds at 500 hPa turning from NW to SW on 13 March (Fig. 10) and by local effects such as valley wind systems and upwinds due to heated mountain flanks.

We further analyzed the mean atmospheric stability calculated as the vertical gradient in equivalent potential temperature θ_e in the presumed source region of air streams 1 and 2 in Northern India from ERA-Interim reanalysis data (not shown). This analysis shows that the inflow of warm and dry air on 11 March associated with the above

ACPD
14, 28105–28146, 2014

mentioned ridge over Northern India resulted in a strong decrease of the PBL height from about 3 to about 1 km. Furthermore, this resulted in a relatively low stability above the PBL up to about 500 hPa. This suggests that vertical spreading of air pollutants up to heights of 5–6 km particularly on and after 11 March, two to three days before the beginning of the observed pollution event over the TP region, is plausible. Once reaching these altitudes, the air pollutants could then be transported to the Himalayas as discussed above for air streams 1 and 2. An exact quantification of the vertical diffusion of air pollutants over the source regions as well as the relative contribution of the synoptic forcing and local effects, however, would require additional model studies and is thus beyond the scope of the current analysis.

3.3.2 Nam Co

Also for the 72 h backward trajectories arriving at Nam Co at 03:00 UTC 16 March 2009, we identify three major air streams (see Fig. 13). We define air stream 1 (28 out of 121 trajectories) as the south-westerly flow which rises to heights of approximately 6000 m a.s.l. on 14 March. Air stream 2 consists of trajectories (54 out of 121) that are advected from the west and stay at altitudes of around 4500 m a.s.l. before following the pathway of air stream 1 over the TP. Air stream 3, finally, originates in the PBL over the foothills of the Himalayas and is advected from the east (39 trajectories).

The basic motion of air parcels in air streams 1 and 2 can again be explained by the synoptic situation. The ridge present on 13 March weakens on 14 March (see Figs. 10 and 14) and a trough associated with the inflow of upper atmospheric cold air from Central Asia forms on the western side of the TP. This leads to westerly and south-westerly winds over northern (air stream 2) and central India (air stream 1), respectively. As the trough moves eastward on 14 March, the wind over much of India turns to a SW direction such that both air stream 1 and 2 are now transported towards the Himalayas (left panel in Fig. 14). Parts of air stream 3 are advected from the east while other parts are trapped in the northern IGP and the adjacent valleys. Winds are generally weak at lower levels during this period. On 15 March, the trough deepens and continues to

ACPD
14, 28105–28146, 2014

move eastward, such that the winds at 500 hPa turn SW and increase in strength (see Fig. 14). This, combined with the heated mountain flanks in the afternoon helps to lift air stream 3 over the Himalayas and onto the TP.

From Fig. 15 it can be seen that air stream 3 is in the PBL most of the time (e.g. from the diurnal temperature variations and high humidity) whereas air streams 1 and 2 are only affected by slow cooling (θ and θ_e). The uplifting of air stream 1 on 14 March can again be explained by northward motion on slanting isentropes in a baroclinic zone.

For both discussed sets of trajectories, a significant amount air mass transport occurs at mid-tropospheric levels (around 500 hPa). This finding is in agreement with the study by Lawrence and Lelieveld (2010) who reported that there appears to be an effective pathway for transport of pollution from IGP to the Himalayas between December and April, especially in the elevated atmospheric layers.

4 Conclusions

The combination of ground and space based remote sensing data together with in-situ observations and NWP model calculations enables a comprehensive assessment of possible transport pathways of polluted air masses, such as ABC, into the very sensitive and remote HTP area.

We investigated a severe pollution episode that occurred on the TP during 13–19 March 2009. This event was selected on the base of AERONET L2 data showing the maximum yearly AOD 500 nm of fine-mode aerosols at Nam Co station in central Tibet. It was also monitored simultaneously at EvK2 station in the high Khumbu Valley in Nepal, where severe pre-monsoonal pollution episodes are observed. The 2009 case study represents the most significant event over the year and contributes with 20 % to the yearly FMF advection to Nam Co.

Further AERONET sites located south of the Himalayas and in Thailand also retrieved very high fine-mode AOD 500 nm during the pollution event in March 2009, representing an episode that occurred on a large scale. This was further supported by

ACPD
14, 28105–28146, 2014

OMI AAOD 500 nm data pointing out the presence of an atmospheric brown cloud with significant amounts of absorbing aerosols over South Asia during 13–19 March 2009. CALIOP high-resolution vertical profiles show aerosols layers "coating" the HTP during the analyzed case study with pollution aerosols extending from the surface up to high tropospheric layers over southern Tibet.

Air mass trajectories were analyzed for severe pollution features observed on the TP during the case study using wind fields from the high-resolution numerical weather prediction model COSMO. The transport of pollution was found to occur along several effective pathways from the IGP and the foothills of the Himalayas to all tropospheric levels over the TP. Approximately two thirds of the analyzed air masses were advected to the TP quasi-isentropically at mid-tropospheric levels and one third was lifted from the PBL south of the Himalayas.

The cross-Himalayan transport of pollution was enabled by the combination of local meteorological patterns such as updrafts near heated mountain flanks and large-scale forcing. Weak zonal winds over the IGP and the Himalayan foothills supported the accumulation of pollution in this region; relatively low stability above the PBL over the IGP permitted for vertical spreading of air pollutants up to the mid-troposphere; local valley wind systems enabled the transport to higher elevations at the southern face of the Himalayas. And finally, the inflow of cold air from higher latitudes lead to the formation of a trough which added a southerly component to the 500 hPa winds, carrying the polluted air masses onto the TP.

Overall, the analyses presented in this study provide an in-depth understanding of cross-Himalayan pollution advection reported in previous works. In particular, we find that ABC and other polluted air masses from the southern side of the Himalayas can traverse the high mountain range not only through the major north–south river valleys but also by being lifted and advected over the Himalayas. Furthermore, we quantify the relative contribution of advection from mid-tropospheric levels over India and the PBL over the Himalayan foothills.

ACPD
14, 28105–28146, 2014

The findings from the meteorological analysis of this case study can be used as a tool for future studies identifying other cross-Himalayan events or studying statistics. Steps that would be involved in such studies might include the quantification of periods with the following characteristics: weak zonal winds at the southern side of the Himalayas and low stability above the PBL (up to about 500 hPa) over the IGP, as well as troughing over the TP followed by a southerly component of the 500 hPa winds over the IGP as the trough passes by.

Chemical models can be used to determine the contribution of specific source regions to polluted air masses that cross the Himalayas. Further observational and modeling studies are urgently needed to identify the chemical speciation and the spatio-temporal distribution of pollutants in the HTP region in order to investigate their climatic and environmental implications, such as possible albedo reductions over snow and ice surfaces resulting from the deposition of absorbing aerosols.

Because of the rapid and effective transport pathway onto the HTP, a reduction in anthropogenic aerosols such as BC would not only be beneficial for human health near the emission sources south of the Himalayas but it would also help to protect the sensitive environments on the Tibetan Plateau.

The Supplement related to this article is available online at doi:10.5194/acpd-14-28105-2014-supplement.

Acknowledgements. This study was supported by the National Natural Science Foundation of China (41225002, 41121001), the Strategic Priority Research Program (B) of the Chinese Academy of Sciences (XDB03030504) and the project "A Sustainable Atmosphere for the Kathmandu Valley" SusKat at the Institute for Advanced Sustainability Studies (IASS), Germany. Our appreciation goes to the many colleagues who have shared their interest and constructive comments for this study, with our special thanks to A. Miltenberger. We thank B. Holben, G. P Gobbi, S. N. Tripathi, G. Leeuw, S. Verma, S. Janjai and their staff for establishing and maintaining the AERONET sites (Nam Co, EVK2-CNR, Kanpur, Pantnagar, Gual_Pahari, Kolkata

ACPD
14, 28105–28146, 2014

and Chiang_Mai_Met_Sta). The CALIOP and OMI data were available form the Atmospheric Science Data Center. BC data from the Ev-K2-CNR SHARE station were generously provided by A. Marinoni.

References

Babu, S. S., Manoj, M., Moorthy, K. K., Gogoi, M. M., Nair, V. S., Kompalli, S. K., Satheesh, S., Niranjan, K., Ramagopal, K., and Bhuyan, P.: Trends in aerosol optical depth over Indian region: potential causes and impact indicators, J. Geophys. Res.-Atmos., 118, 11794–11806, doi:10.1002/2013JD020507, 2013.

Baldauf, M., Seifert, A., Förstner, J., Majewski, D., Raschendorfer, M., and Reinhardt, T.: Operational convective-scale numerical weather prediction with the COSMO Model: description and sensitivities, Mon. Weather Rev., 139, 3887–3905, doi:10.1175/MWR-D-10-05013.1, 2011.

Bolch, T., Kulkarni, A., Kaab, A., Huggel, C., Paul, F., Cogley, J. G., Frey, H., Kargel, J. S., Fujita, K., Scheel, M., Bajracharya, S., and Stoffel, M.: The state and fate of Himalayan glaciers, Science, 336, 310–314, doi:10.1126/science.1215828, 2012.

Bonasoni, P., Laj, P., Marinoni, A., Sprenger, M., Angelini, F., Arduini, J., Bonafè, U., Calzolari, F., Colombo, T., Decesari, S., Di Biagio, C., di Sarra, A. G., Evangelisti, F., Duchi, R., Facchini, MC., Fuzzi, S., Gobbi, G. P., Maione, M., Panday, A., Roccato, F., Sellegri, K., Venzac, H., Verza, GP., Villani, P., Vuillermoz, E., and Cristofanelli, P.: Atmospheric Brown Clouds in the Himalayas: first two years of continuous observations at the Nepal Climate Observatory-Pyramid (5079 m), Atmos. Chem. Phys., 10, 7515–7531, doi:10.5194/acp-10-7515-2010, 2010.

Bond, T., Doherty, S., Fahey, D., Forster, P., Berntsen, T., DeAngelo, B., Flanner, M., Ghan, S., Kärcher, B., and Koch, D.: Bounding the role of black carbon in the climate system: a scientific assessment, J. Geophys. Res.-Atmos., 118, 5380–5552, 2013.

Cao, J., Tie, X., Xu, B., Zhao, Z., Zhu, C., Li, G., and Liu, S.: Measuring and modeling black carbon (BC) contamination in the SE Tibetan Plateau, J. Atmos. Chem., 67, 45–60, 2011.

Cong, Z.: Individual particle analysis of atmospheric aerosols at Nam Co, Tibetan Plateau, Aerosol Air Qual. Res., 9 , 323–331, doi:10.4209/aaqr.2008.12.0064, 2009.

ACPD
14, 28105–28146, 2014

Decesari, S., Facchini, M. C., Carbone, C., Giulianelli, L., Rinaldi, M., Finessi, E., Fuzzi, S., Marinoni, A., Cristofanelli, P., Duchi, R., Bonasoni, P., Vuillermoz, E., Cozic, J., Jaffrezo, J. L., and Laj, P.: Chemical composition of PM_{10} and PM_1 at the high-altitude Himalayan station Nepal Climate Observatory-Pyramid (NCO-P) (5079 m a.s.l.), Atmos. Chem. Phys., 10, 4583–4596, doi:10.5194/acp-10-4583-2010, 2010.

Dey, S. and Di Girolamo, L.: A climatology of aerosol optical and microphysical properties over the Indian subcontinent from 9 years (2000–2008) of Multiangle Imaging Spectroradiometer (MISR) data, J. Geophys. Res., 115, D15204, doi:10.1029/2009jd013395, 2010.

Dubovik, O. and King, M. D.: A flexible inversion algorithm for retrieval of aerosol optical properties from Sun and sky radiance measurements, J. Geophys. Res.-Atmos., 105, 20673–20696, 2000.

Dubovik, O., Smirnov, A., Holben, B., King, M., Kaufman, Y., Eck, T., and Slutsker, I.: Accuracy assessments of aerosol optical properties retrieved from Aerosol Robotic Network (AERONET) Sun and sky radiance measurements, J. Geophys. Res.-Atmos., 105, 9791–9806, 2000.

Eck, T. F., Holben, B. N., Reid, J. S., Dubovik, O., Smirnov, A., O'Neill, N. T., Slutsker, I., and Kinne, S.: Wavelength dependence of the optical depth of biomass burning, urban, and desert dust aerosols, J. Geophys. Res.-Atmos., 104, 31333–31349, doi:10.1029/1999jd900923, 1999.

Eck, T., Holben, B., Sinyuk, A., Pinker, R., Goloub, P., Chen, H., Chatenet, B., Li, Z., Singh, R., and Tripathi, S.: Climatological aspects of the optical properties of fine/coarse mode aerosol mixtures, J. Geophys. Res.-Atmos., 115, D19205, doi:10.1029/2010JD014002, 2010.

Engling, G. and Gelencser, A.: Atmospheric brown clouds: from local air pollution to climate change, Elements, 6, 223–228, doi:10.2113/gselements.6.4.223, 2010.

Engling, G., Zhang, Y.-N., Chan, C.-Y., Sang, X.-F., Lin, M., Ho, K.-F., Li, Y.-S., Lin, C.-Y., and Lee, J. J.: Characterization and sources of aerosol particles over the southeastern Tibetan Plateau during the Southeast Asia biomass-burning season, Tellus B, 63, 117–128, doi:10.1111/j.1600-0889.2010.00512.x, 2011.

Flanner, M. G., Zender, C. S., Randerson, J. T., and Rasch, P. J.: Present-day climate forcing and response from black carbon in snow, J. Geophys. Res., 112, D11202, doi:10.1029/2006JD008003, 2007.

Fleming, Z. L., Monks, P. S., and Manning, A. J.: Review: Untangling the influence of air-mass history in interpreting observed atmospheric composition, Atmos. Res., 104, 1–39, 2012.

ACPD
14, 28105–28146, 2014

Gautam, R., Hsu, N. C., and Lau, K. M.: Premonsoon aerosol characterization and radiative effects over the Indo-Gangetic Plains: implications for regional climate warming, J. Geophys. Res., 115, D17208, doi:10.1029/2010jd013819, 2010.

Gautam, R., Hsu, N. C., Tsay, S. C., Lau, K. M., Holben, B., Bell, S., Smirnov, A., Li, C., Hansell, R., Ji, Q., Payra, S., Aryal, D., Kayastha, R., and Kim, K. M.: Accumulation of aerosols over the Indo-Gangetic plains and southern slopes of the Himalayas: distribution, properties and radiative effects during the 2009 pre-monsoon season, Atmos. Chem. Phys., 11, 12841–12863, doi:10.5194/acp-11-12841-2011, 2011.

Holben, B., Eck, T., Slutsker, I., Tanre, D., Buis, J., Setzer, A., Vermote, E., Reagan, J., Kaufman, Y., and Nakajima, T.: AERONET – A federated instrument network and data archive for aerosol characterization, Remote Sens. Environ., 66, 1–16, 1998.

Immerzeel, W. W., van Beek, L. P., and Bierkens, M. F.: Climate change will affect the Asian water towers, Science, 328, 1382–1385, doi:10.1126/science.1183188, 2010.

Jacobson, M. Z.: Strong radiative heating due to the mixing state of black carbon in atmospheric aerosols, Nature, 409, 695–697, 2001.

Kang, S., Xu, Y., You, Q., Flügel, W.-A., Pepin, N., and Yao, T.: Review of climate and cryospheric change in the Tibetan Plateau, Environ. Res. Lett., 5, 015101, doi:10.1088/1748-9326/5/1/015101, 2010.

Kaspari, S. D., Schwikowski, M., Gysel, M., Flanner, M. G., Kang, S., Hou, S., and Mayewski, P. A.: Recent increase in black carbon concentrations from a Mt. Everest ice core spanning 1860–2000 AD, Geophys. Res. Lett., 38, L04703, doi:10.1029/2010gl046096, 2011.

Kehrwald, N. M., Thompson, L. G., Tandong, Y., Mosley-Thompson, E., Schotterer, U., Alfimov, V., Beer, J., Eikenberg, J., and Davis, M. E.: Mass loss on Himalayan glacier endangers water resources, Geophys. Res. Lett., 35, L22503, doi:10.1029/2008GL035556, 2008.

Kopacz, M., Mauzerall, D. L., Wang, J., Leibensperger, E. M., Henze, D. K., and Singh, K.: Origin and radiative forcing of black carbon transported to the Himalayas and Tibetan Plateau, Atmos. Chem. Phys., 11, 2837–2852, doi:10.5194/acp-11-2837-2011, 2011.

Lau, W. K. M., Kim, M.-K., Kim, K.-M., and Lee, W.-S.: Enhanced surface warming and accelerated snow melt in the Himalayas and Tibetan Plateau induced by absorbing aerosols, Environ. Res. Lett., 5, 025204, doi:10.1088/1748-9326/5/2/025204, 2010.

Lawrence, M. G. and Lelieveld, J.: Atmospheric pollutant outflow from southern Asia: a review, Atmos. Chem. Phys., 10, 11017–11096, doi:10.5194/acp-10-11017-2010, 2010.

ACPD
14, 28105–28146, 2014

Lu, Z., Streets, D. G., Zhang, Q., and Wang, S.: A novel back-trajectory analysis of the origin of black carbon transported to the Himalayas and Tibetan Plateau during 1996–2010, Geophys. Res. Lett., 39, L01809, doi:10.1029/2011gl049903, 2012.

Ma, Y., Wang, Y., Wu, R., Hu, Z., Yang, K., Li, M., Ma, W., Zhong, L., Sun, F., Chen, X., Zhu, Z., Wang, S., and Ishikawa, H.: Recent advances on the study of atmosphere-land interaction observations on the Tibetan Plateau, Hydrol. Earth Syst. Sci., 13, 1103–1111, doi:10.5194/hess-13-1103-2009, 2009.

Marinoni, A., Cristofanelli, P., Laj, P., Duchi, R., Calzolari, F., Decesari, S., Sellegri, K., Vuillermoz, E., Verza, G. P., Villani, P., and Bonasoni, P.: Aerosol mass and black carbon concentrations, a two year record at NCO-P (5079 m, Southern Himalayas), Atmos. Chem. Phys., 10, 8551–8562, doi:10.5194/acp-10-8551-2010, 2010.

Marinoni, A., Cristofanelli, P., Laj, P., Duchi, R., Putero, D., Calzolari, F., Landi, T. C., Vuillermoz, E., Maione, M., and Bonasoni, P.: High black carbon and ozone concentrations during pollution transport in the Himalayas: five years of continuous observations at NCO-P global GAW station, J. Environ. Sci.-China, 25, 1618–1625, doi:10.1016/S1001-0742(12)60242-3, 2013.

Ming, J., Wang, P., Zhao, S., and Chen, P.: Disturbance of light-absorbing aerosols on the albedo in a winter snowpack of Central Tibet, J. Environ. Sci.-China, 25, 1601–1607, doi:10.1016/s1001-0742(12)60220-4, 2013.

Moorthy, K. K., Sreekanth, V., Prakash Chaubey, J., Gogoi, M. M., Suresh Babu, S., Kumar Kompalli, S., Bagare, S. P., Bhatt, B. C., Gaur, V. K., Prabhu, T. P., and Singh, N. S.: Fine and ultrafine particles at a near–free tropospheric environment over the high-altitude station Hanle in the Trans-Himalaya: new particle formation and size distribution, J. Geophys. Res., 116, D20212, doi:10.1029/2011jd016343, 2011.

O'Neill, N. T.: Spectral discrimination of coarse and fine mode optical depth, J. Geophys. Res., 108, 4559, doi:10.1029/2002jd002975, 2003.

Prabha, T. V., Karipot, A., Axisa, D., Kumari, B. P., Maheskumar, R. S., Konwar, M., Kulkarni, J. R., and Goswami, B. N.: Scale interactions near the foothills of Himalayas during CAIPEEX, J. Geophys. Res.-Atmos., 117, D10203, doi:10.1029/2011jd016754, 2012.

Qian, Y., Flanner, M. G., Leung, L. R., and Wang, W.: Sensitivity studies on the impacts of Tibetan Plateau snowpack pollution on the Asian hydrological cycle and monsoon climate, Atmos. Chem. Phys., 11, 1929–1948, doi:10.5194/acp-11-1929-2011, 2011.

ACPD
14, 28105–28146, 2014

Ramanathan, V. and Carmichael, G.: Global and regional climate changes due to black carbon, Nat. Geosci., 1, 221–227, 2008.
Ramanathan, V., Li, F., Ramana, M. V., Praveen, P. S., Kim, D., Corrigan, C. E., Nguyen, H., Stone, E. A., Schauer, J. J., Carmichael, G. R., Adhikary, B., and Yoon, S. C.: Atmospheric brown clouds: hemispherical and regional variations in long-range transport, absorption, and radiative forcing, J. Geophys. Res., 112, D22S21, doi:10.1029/2006jd008124, 2007a.
Ramanathan, V., Ramana, M. V., Roberts, G., Kim, D., Corrigan, C., Chung, C., and Winker, D.: Warming trends in Asia amplified by brown cloud solar absorption, Nature, 448, 575–578, doi:10.1038/nature06019, 2007b.
Škerlak, B., Sprenger, M., and Wernli, H.: A global climatology of stratosphere–troposphere exchange using the ERA-Interim data set from 1979 to 2011, Atmos. Chem. Phys., 14, 913–937, doi:10.5194/acp-14-913-2014, 2014.
Smirnov, A., Holben, B., Eck, T., Dubovik, O., and Slutsker, I.: Cloud-screening and quality control algorithms for the AERONET database, Remote Sens. Environ., 73, 337–349, 2000.
Thompson, L. G., Yao, T., Mosley-Thompson, E., Davis, M., Henderson, K., and Lin, P.-N.: A high-resolution millennial record of the South Asian monsoon from Himalayan ice cores, Science, 289, 1916–1919, 2000.
Torres, O., Tanskanen, A., Veihelmann, B., Ahn, C., Braak, R., Bhartia, P. K., Veefkind, P., and Levelt, P.: Aerosols and surface UV products from Ozone Monitoring Instrument observations: an overview, J. Geophys. Res.-Atmos., 112, D24S47, doi:10.1029/2007JD008809, 2007.
Wernli, B. H. and Davies, H. C.: A Lagrangian-based analysis of extratropical cyclones, I: The method and some applications, Q. J. Roy. Meteor. Soc., 123, 467–489, 1997.
Winker, D. M., Vaughan, M. A., Omar, A., Hu, Y., Powell, K. A., Liu, Z., Hunt, W. H., and Young, S. A.: Overview of the CALIPSO mission and CALIOP data processing algorithms, J. Atmos. Ocean. Tech., 26, 2310–2323, 2009.
Xia, X., Zong, X., Cong, Z., Chen, H., Kang, S., and Wang, P.: Baseline continental aerosol over the central Tibetan plateau and a case study of aerosol transport from South Asia, Atmos. Environ., 45, 7370–7378, doi:10.1016/j.atmosenv.2011.07.067, 2011.
Xu, B., Cao, J., Hansen, J., Yao, T., Joswia, D. R., Wang, N., Wu, G., Wang, M., Zhao, H., Yang, W., Liu, X., and He, J.: Black soot and the survival of Tibetan glaciers, P. Natl. Acad. Sci. USA, 106, 22114–22118, doi:10.1073/pnas.0910444106, 2009.

ACPD
14, 28105–28146, 2014

Yao, T., Thompson, L., Yang, W., Yu, W., Gao, Y., Guo, X., Yang, X., Duan, K., Zhao, H., and Xu, B.: Different glacier status with atmospheric circulations in Tibetan Plateau and surroundings, Nat. Clim. Change, 2, 663–667, 2012.

Ye, D.-Z. and Wu, G.-X.: The role of the heat source of the Tibetan Plateau in the general circulation, Meteorol. Atmos. Phys., 67, 181–198, 1998.

Zhao, S., Ming, J., Sun, J., and Xiao, C.: Observation of carbonaceous aerosols during 2006–2009 in Nyainqentanglha Mountains and the implications for glaciers, Environ. Sci. Pollut. Res. Int., 20, 5827–5838, doi:10.1007/s11356-013-1548-6, 2013.

ACPD
14, 28105–28146, 2014

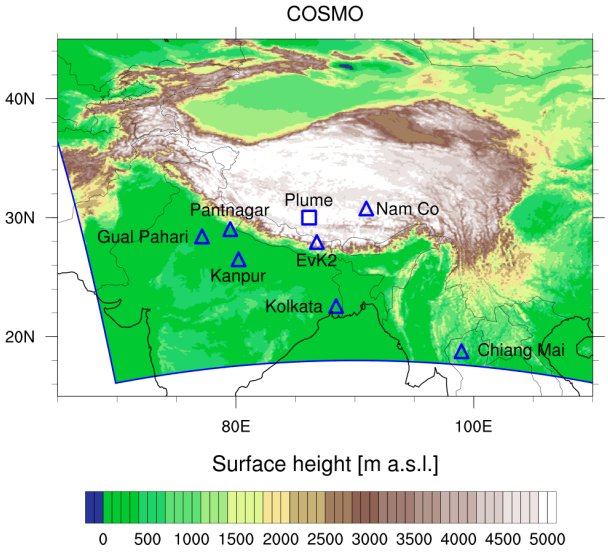

Figure 1. Topography of the Indian subcontinent and the Tibetan Plateau in COSMO. Blue triangles indicate the AERONET stations used in this study and the blue square shows the observed location of a pollution plume.

ACPD
14, 28105–28146, 2014

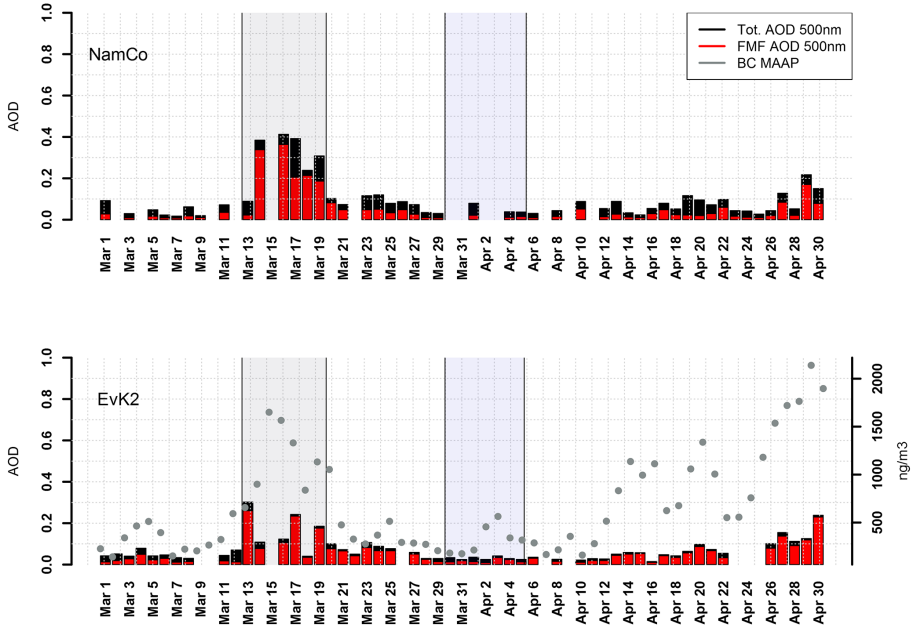

Figure 2. AERONET AOD time series. Red bars indicate the fine-mode fraction (FMF) of the total aerosol optical depth (AOD) at 500 nm (black columns). Blank dates are days without data. Gray circles indicate black carbon measurements from Multi-Angle Absorption Photometer (MAAP) at EvK2. The pollution event analyzed in this study (13–19 March 2009) is highlighted in gray and the cleaner period (30 March–5 April 2009) is highlighted in blue.

ACPD
14, 28105–28146, 2014

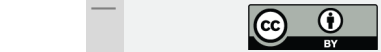

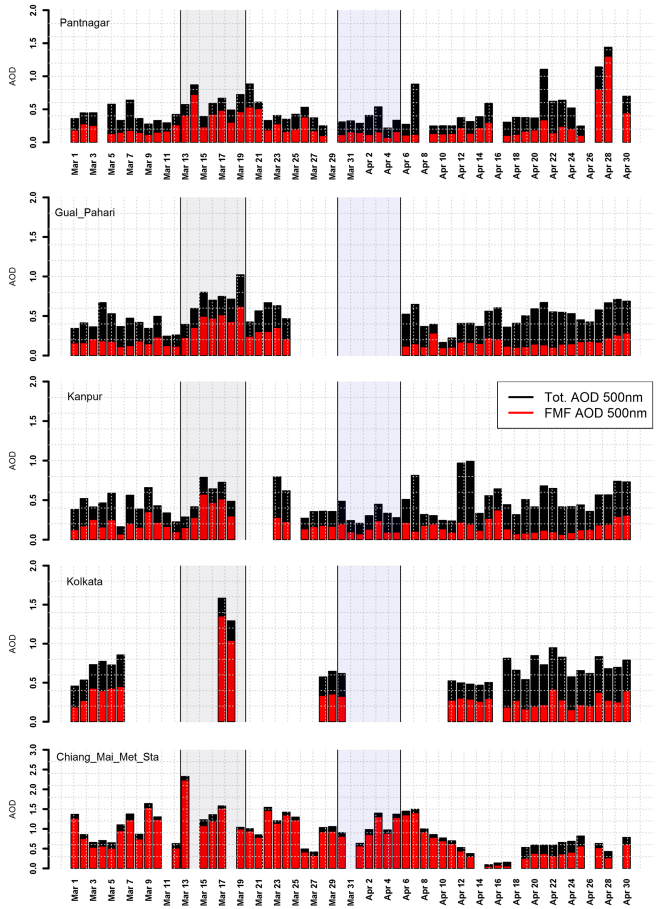

Figure 3. Same as Fig. 2 for AERONET stations over the IGP and in Thailand.

ACPD
14, 28105–28146, 2014

Atmospheric brown clouds reach the Tibetan Plateau by crossing the Himalayas

Z. L. Lüthi et al.

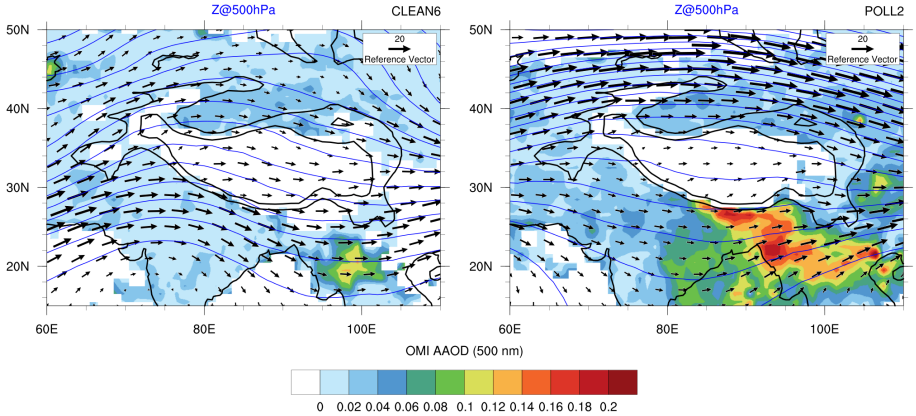

Figure 4. OMI AAOD (500 nm, colored), geopotential height (contours, 250 m spacing) and wind (reference arrow, 20 m s^{-1}) at 500 hPa from ERA-Interim averaged over: **(a)** the pollution event 13–19 March 2009, and for **(b)** a cleaner 7 day period between 30 March and 5 April 2009.

ACPD
14, 28105–28146, 2014

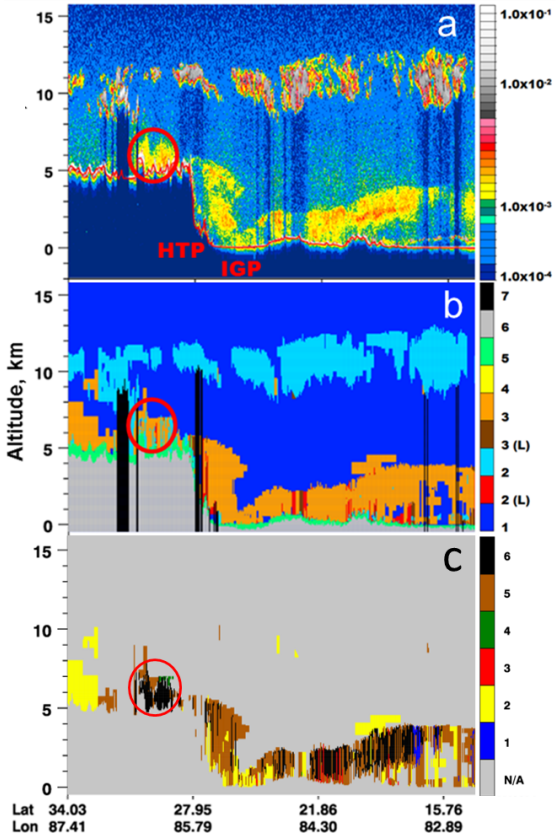

Figure 5. (a) CALIOP vertical profile at 20:30 UTC 13 March 2009 showing the color-coded total attenuated backscatter lidar return signal at 532 nm with green, yellow, and red indicating aerosols at low, medium and high concentrations, respectively; **(b)** cloud-aerosol output, with 1 clear air, 2 cloud, 3 aerosol, 4 stratospheric layer, 5 surface, 6 subsurface and 7 totally attenuated; **(c)** aerosol subtype profiles with 1 clean marine, 2 dust, 3 polluted continental, 4 clean continental, 5 polluted dust and 6 smoke. Red circles mark the plume over the TP.

ACPD
14, 28105–28146, 2014

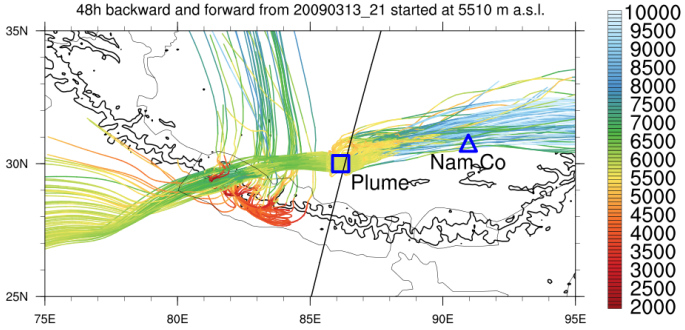

Figure 6. Trajectories (48 h backward and forward) started near the observed high aerosol concentrations ("Plume", blue square) at 21:00 UTC 13 March 2009 from an altitude of 5510 m a.s.l. Height along the trajectories is color coded (in m a.s.l.), black lines show the orography (2000 and 4000 m a.s.l. contour lines), the blue triangle is Nam Co station and the thick solid black line shows the CALIOP transect.

ACPD
14, 28105–28146, 2014

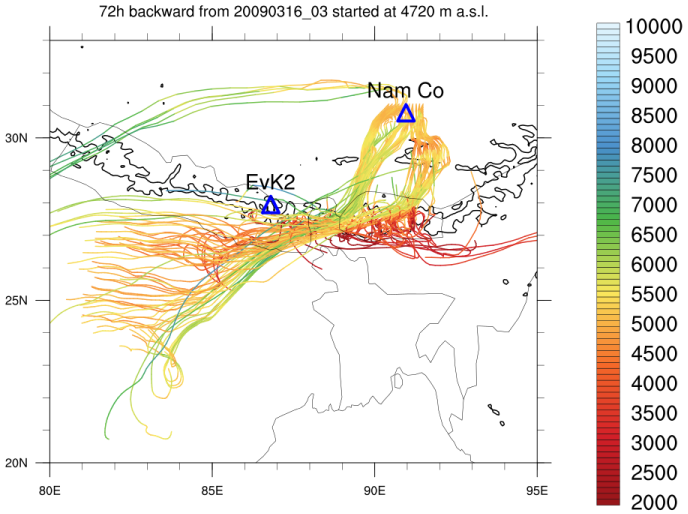

Figure 7. Trajectories (72 h backward) started near Nam Co (blue triangle) at 03:00 UTC 16 March 2009 from an altitude of 4720 m a.s.l. Height along the trajectories is color coded (in m a.s.l.), black lines show orography (2000 and 4000 m a.s.l. contour lines), and the other blue triangle is EvK2 station.

ACPD
14, 28105–28146, 2014

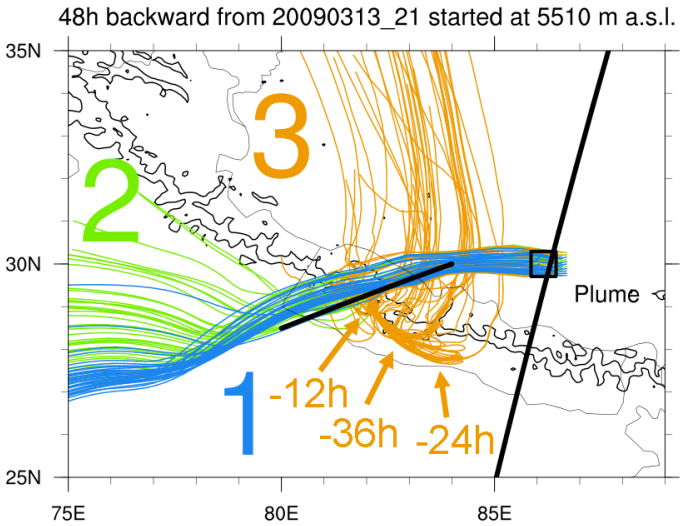

Figure 8. Same as in Fig. 6 with three categories of backward trajectories: air stream 1 for trajectories above 5500 m a.s.l. over the IGP, air stream 2 otherwise and air stream 3 for trajectories originating over the TP. The time along air stream 3 is indicated for 12, 24 and 36 h prior to reaching the plume location.

ACPD
14, 28105–28146, 2014

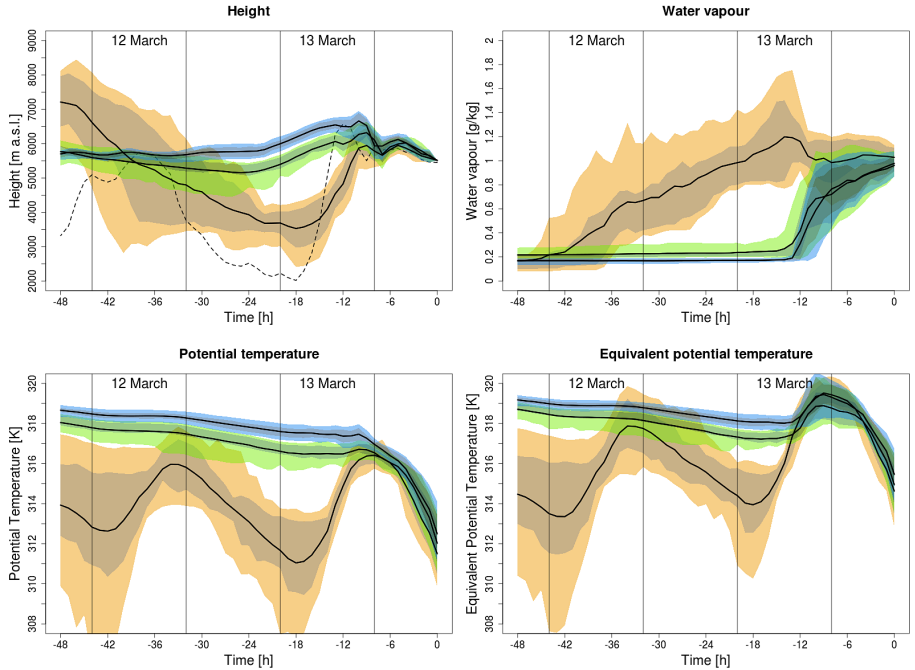

Figure 9. Temporal evolution of height, water vapor (Qv), potential temperature (θ) and equivalent potential temperature (θ_e) for the 48 h backward trajectories started at 21:00 UTC 13 March 2009 near the plume location at 5510 m a.s.l. Blue, green and orange colors show air streams 1, 2 and 3 as described in the text, respectively (cf. Fig. 8). Black lines show median values at every time step and the shading indicates 10, 25, 75 and 90 percentiles (121 trajectories). The thin vertical lines indicate 06:00 and 18:00 LT as an approximation for day- and nighttime. The dashed line in the top left panel shows the median height of the PBL top along air stream 3 (orange).

ACPD
14, 28105–28146, 2014

Atmospheric brown clouds reach the Tibetan Plateau by crossing the Himalayas

Z. L. Lüthi et al.

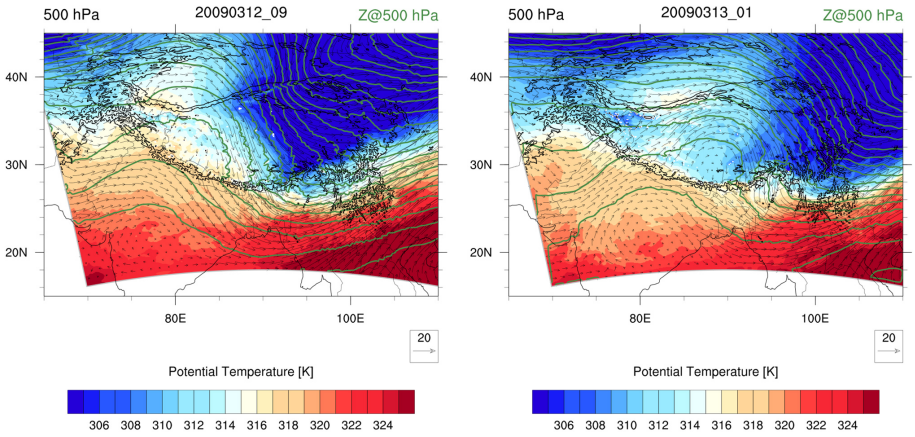

Figure 10. Geopotential height (green lines, contour intervals 250 m) and potential temperature (colored, in K) at 09:00 UTC 12 March 2009 (left panel) and 01:00 UTC 13 March 2009 (right panel). Horizontal wind at 500 hPa is indicated with arrows (reference arrow 20 m s^{-1}).

ACPD
14, 28105–28146, 2014

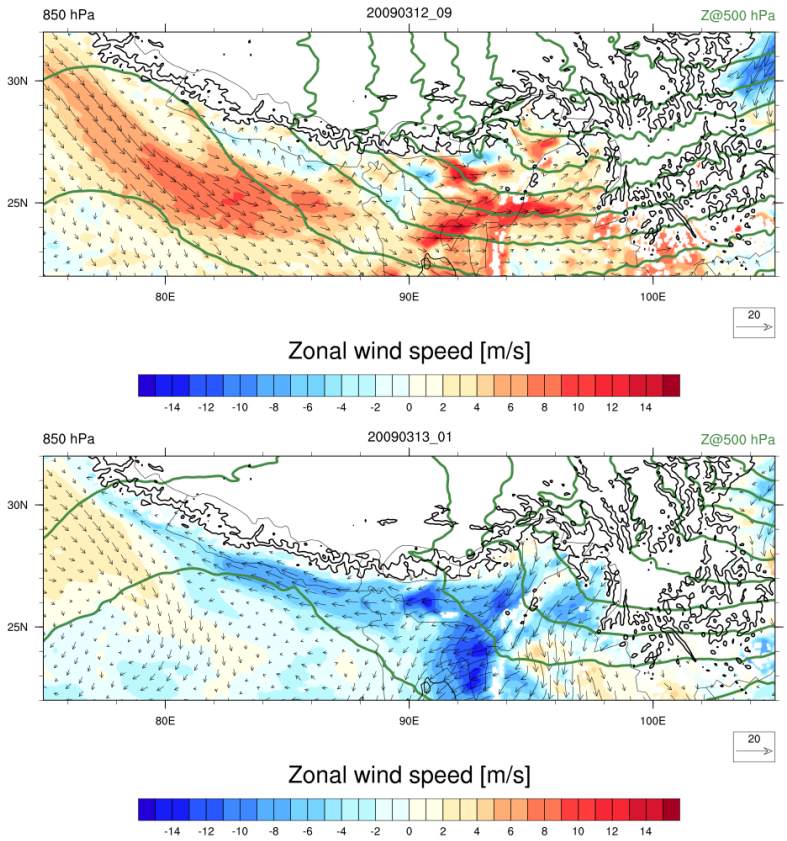

Figure 11. Geopotential height at 500 hPa (green lines, contour intervals 250 m) and zonal wind speed (colored, in $m\,s^{-1}$) at 850 hPa at 09:00 UTC 12 March 2009 (top panel) and at 01:00 UTC 13 March 2009 (bottom panel). Horizontal wind at 850 hPa is indicated with arrows (reference arrow $20\,m\,s^{-1}$).

ACPD
14, 28105–28146, 2014

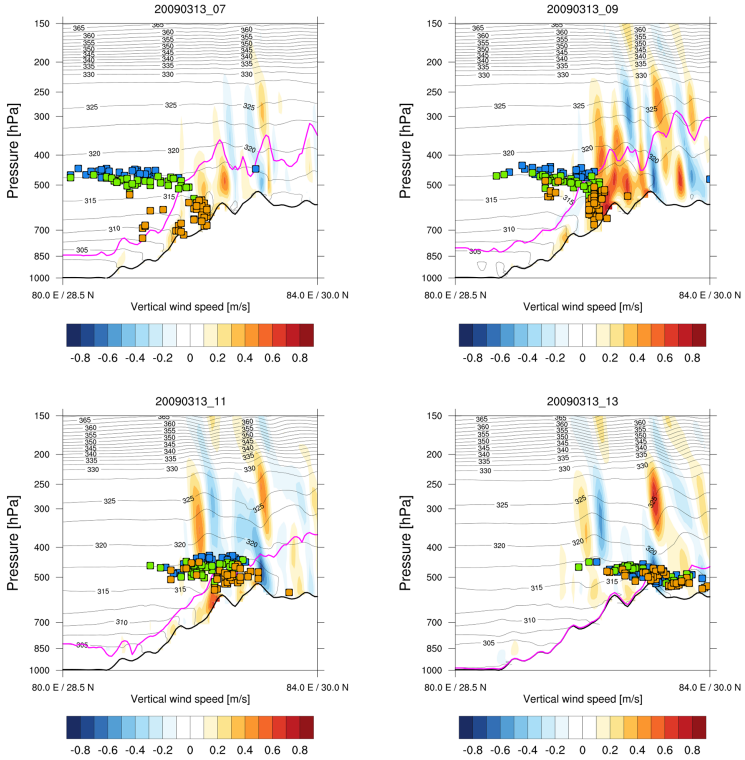

Figure 12. Vertical cross-sections along the mean direction of transport (thick black line in Fig. 8) at 07:00, 09:00, 11:00 and 13:00 UTC 13 March 2009. Colored contours show vertical wind speed ($m\,s^{-1}$), thin black lines are isentropes (K), thick black line is the surface and the magenta line shows the PBL top as calculated by COSMO via a Bulk-Richardson Number method. Trajectory positions are zonally projected onto the cross-section; blue, green and orange filled squares represent air stream 1, 2 and 3, respectively.

ACPD
14, 28105–28146, 2014

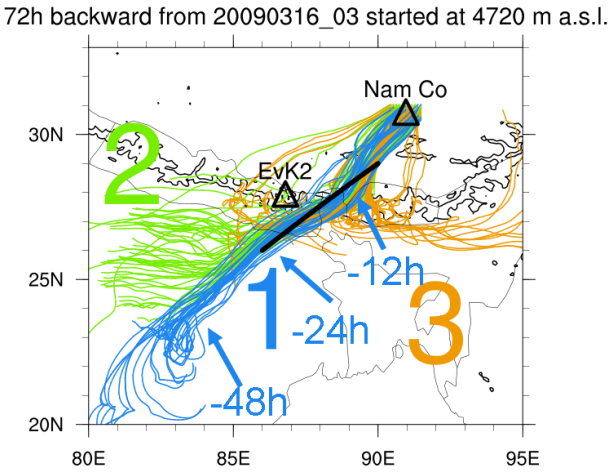

Figure 13. Same as Fig. 7 with three trajectories categories: air stream 1 for south-westerly flow rising to heights around 6000 m a.s.l. on 14 March; air stream 2 advecting from the west at heights around 4500 m a.s.l. and air stream 3 originating in the PBL. The time along air stream 1 is indicated for 12, 24 and 48 h prior to reaching Nam Co.

ACPD
14, 28105–28146, 2014

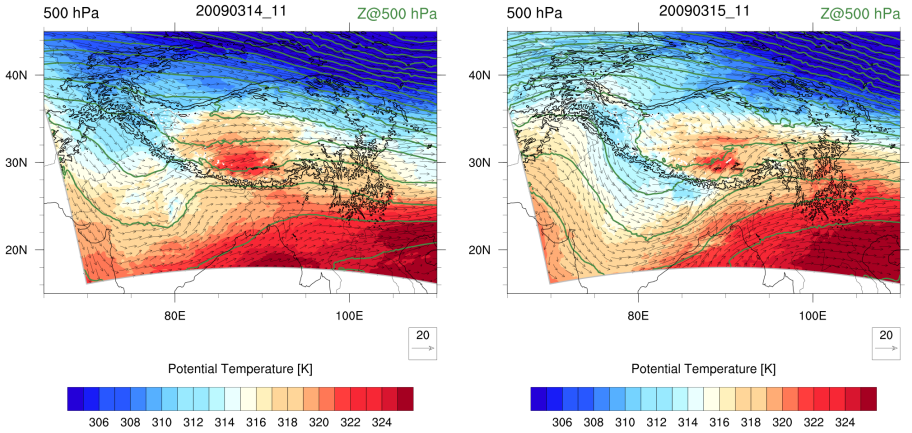

Figure 14. Geopotential height (green lines, contour intervals 250 m) and potential temperature (colored, in K) at 11:00 UTC 14 March 2009 (left panel) and 11:00 UTC 15 March 2009 (right panel). Horizontal wind at 500 hPa is indicated with arrows (reference arrow 20 m s^{-1}).

ACPD
14, 28105–28146, 2014

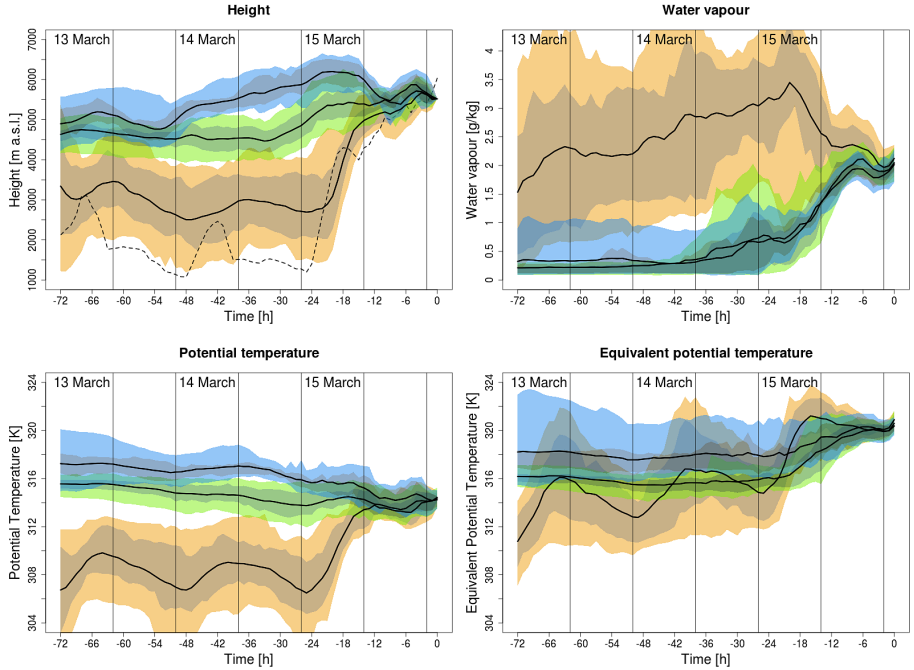

Figure 15. Same as Fig. 9 but for the 72 h backward trajectories started at 03:00 UTC 16 March 2009 in the vicinity of Nam Co at 4720 m a.s.l.

ACPD
14, 28105–28146, 2014